



Additive Manufacturing of Polyaniline Blends for Lightweight Structures with Tunable Conductivity

| | |
|-------------------------------|---|
| Journal: | <i>Journal of Materials Chemistry C</i> |
| Manuscript ID | TC-ART-10-2022-004183.R1 |
| Article Type: | Paper |
| Date Submitted by the Author: | 13-Jan-2023 |
| Complete List of Authors: | DiTullio, Brandon ; Georgia Institute of Technology Kuang, Xiao; Georgia Tech Österholm, Anna; Georgia Institute of Technology, Lang, Augustus; Georgia Institute of Technology, Chemistry and Biochemistry, Materials Science and Engineering Kinlen, Patrick; retired Qi, H.; Georgia Institute of Technology, School of Mechanical Engineering Stingelin, Natalie; Georgia Institute of Technology, Materials Science and Engineering Reynolds, John; Georgia Institute of Technology, Chemistry and Biochemistry, Materials Science and Engineering |
| | |

Additive Manufacturing of Polyaniline Blends for Lightweight Structures with Tunable Conductivity

Brandon T. DiTullio,^a Xiao Kuang,^b Anna M. Österholm,^a Augustus W. Lang,^c Patrick J. Kinlen,^d Natalie Stingelin,^{c,e} H. Jerry Qi,^b John R. Reynolds^{a,c}*

^a School of Chemistry and Biochemistry, Center for Organic Photonics and Electronics, Georgia Tech Polymer Network, Georgia Institute of Technology, Atlanta, GA 30332, USA.

^b The George W. Woodruff School of Mechanical Engineering, Georgia Institute of Technology, Atlanta, GA 30332, USA

^c School of Materials Science and Engineering, Center for Organic Photonics and Electronics, Georgia Tech Polymer Network, Georgia Institute of Technology, Atlanta, GA 30332, USA

^d 1348 Remington Oaks Terr., Fenton, MO 63026, USA

^e School of Chemical and Biomolecular Engineering, Georgia Institute of Technology, Atlanta, GA 30332, USA

Corresponding author: reynolds@chemistry.gatech.edu

Abstract

Printable feedstocks that can produce lightweight, robust, and ductile structures with tunable and switchable conductivity are of considerable interest for numerous application spaces. Combining the specific properties of commodity thermoplastics with the unique electrical and redox properties of conducting polymers (CPs) presents new opportunities for the field of printed (bio)electronics. Here, we report on the direct ink write (DIW) printing of ink formulations based on polyaniline-dinonylnaphthalene sulfonic acid (PANI-DNNSA), which has been synthesized in bulk quantities (~400 g). DNNSA imparts solubility to PANI up to 50 mg/mL, which allows the use of various additives to tune the rheological behavior of the inks without significantly compromising the electrical properties of the printed structures, which reach conductivities in the range of $< 10^{-7} - 10^0 \text{ S cm}^{-1}$ as a function of ink formulation and post treatment used. Fumed silica (FS) and ultra-high molecular weight polystyrene (UHMW-PS) additives are leveraged to endow printability and shape retention to inks, as well as to compare the use of traditional rheological modifiers with commodity thermoplastics on CP feedstocks for tailored DIW printing. We show that the incorporation of UHMW-PS into these ink formulations is critical for obtaining high crack resistance in printed structures. This work serves as a guide for future ink designs of CPs with commodity thermoplastics and their subsequent DIW printing to yield conductive architectures and devices for various applications.

Introduction

Ink formulations that enable additive manufacturing (AM) to produce structures having tunable and switchable electronic properties are of considerable interest for numerous applications such as electrostatic dissipation (ESD),¹ electromagnetic interference (EMI) shielding,^{2,3} wearable electronics (sensing),⁴ tissue engineering,⁵ soft robotics,⁶ and Joule heating.⁷ In addition, materials capable of effectively storing and transporting electrons and/or ions are needed for energy-related applications such as Li-ion batteries⁸ and supercapacitors.⁹ Printing these materials into shapes, such as grids, strain gauges, and thermocouple interfaces,

would be valuable for measuring temperature, strain, and strain rate of materials.^{10,11} These types of advances require the development and understanding of new AM methodologies and the rational design of low-cost, multifunctional material feedstocks.

Conducting polymers (CPs) are a versatile class of materials that can access a large range of conductivity values (10^{-10} - 10^3 S cm^{-1}) and that have unique redox chemistry associated with mixed ionic/electronic transport.¹²⁻¹⁴ Additionally, unlike inorganic materials such as silver and copper, CPs are lightweight, resistant to corrosion, and solution processable. The solution processability of CPs promises continuous and high throughput printing *via* direct ink write (DIW), which opens the opportunity to produce highly customized/complex structures. Traditional manufacturing is capable of producing 3D structures at large volumes using injection molding, but producing useful quantities of highly complex structures that require customization or numerous processing steps will require inexpensive AM techniques (such as DIW) to reach economies of scale.¹⁵

To date, two notable CPs, poly(3,4-ethylenedioxythiophene) (PEDOT)^{16,17} and polyaniline (PANI),^{18,19} have been investigated as material feedstock alternatives for additive manufacturing (AM). For the former, poly(styrene sulfonate) (PSS), a dopant used in the synthesis of the macromolecular salt, PEDOT:PSS, enables stable dispersions in water, which allowed for careful formulation for DIW printing structures with high conductivity (> 100 S cm^{-1}), low modulus (< 1 MPa), high resolution (> 30 μm), and high aspect ratio (> 20 layers).¹⁶ However, ink formulation of aqueous PEDOT:PSS solutions requires cryogenic freezing, followed by lyophilization, and subsequent redispersion, which, in addition to high monomer costs, could pose logistical and economical challenges to feedstock production on the industrial scale. In this regard, we find that PANI-based materials can offer advantages over PEDOT-PSS due to its potential for organic solvent processability that allows for its mixing with thermoplastics and other additives that require organic processing. PANI is straightforward and easy to synthesize, offers unique protonation (doping) chemistry, can be blended in solution

with a variety of ink additives, has tunable and switchable conductivity, along with satisfactory environmental stability and biocompatibility.²⁰⁻²² Kinlen et al. have developed an emulsion polymerization technique for PANI doped with dinonylnaphthalenesulfonic acid (DNNSA) where the intercalation of the bulky DNNSA dopant molecules between PANI chains successfully disrupts aggregation and promotes polymer dissolution, affording unusually high solubility (capable of filtration with submicron pore sizes at concentrations > 50 mg/mL) in a wide range of apolar organic solvents (e.g., toluene, xylenes, hexanes, etc.).²³ They also showed that post-treatments with low-molecular weight alcohols such as isopropanol (IPA), *n*-butanol (BuOH), and butyl CELLOSOLVE™ (2-butoxyethanol) are able to remove excess DNNSA ions and promote ordering of PANI chains, thereby increasing the conductivity of the resulting films by ~8 orders of magnitude, up to 200 S cm⁻¹.²⁴**Error! Bookmark not defined.** The enhanced solubility and high/tunable solid-state conductivity of PANI-DNNSA make it an excellent candidate for incorporation into ink formulations for DIW printing. In fact, printed PANI-DNNSA has already been tested as an active material for structural health monitors on aircrafts.²⁵

In order to DIW print CP-based materials, ink formulations must be suitable for extrusion through a nozzle, which requires specific rheological properties that confer sufficient shear-thinning character, while also promoting shape retention. For extrusion, the required shear thinning characteristics are generally afforded by apparent viscosities of lower than 10⁴ Pa·s at a shear rate = 10⁻¹ s⁻¹ and 10¹ Pa·s at a shear rate = 10² s⁻¹.²⁶⁻²⁹ For adequate shape retention, successful DIW ink formulations typically have a zero-shear viscosity of ≈ 10³-10⁵ Pa·s, yield stresses of ≈ 10¹-10³ Pa, and storage moduli of ≈ 10³-10⁵ Pa.³⁰⁻³² Many polymer solutions, including those of CPs, are unable to achieve these rheological requirements, and additives are often required to tune the rheological properties of the inks. One common approach is to add fumed silica (FS), which is a well-known 3D-printing additive that is composed of individual primary silica particles (ranging from 5-400 nm) that can assemble into

larger three-dimensional particle networks with at least two fractal dimensions (radius of gyration, $R_g \approx 10 \mu\text{m}$) under low-shear conditions, increasing the viscosity of the solution.³³ Upon shearing FS colloidal suspensions at increasing shear rates, the average radius of FS clusters, and consequently the viscosity, decreases until the primary nanoparticles are fully fragmented into solution. The use of thermoplastic commodity-polymer additives in AM^{34,35} is, however, less explored despite the fact that blending CPs with high-density polyethylene (HDPE), poly(methyl methacrylate) (PMMA) and polystyrene (PS) have been successfully used in the fabrication of thin-film transistors and organic solar cells, leading to an enhancement of environmental stability, film formation, and mechanical robustness without compromising charge transport properties.³⁶⁻³⁸

In this work, we focus on a PANI-DNNSA ink specifically designed to impart DIW printability and, once printed, to afford shape retention for crack-resistant, electrically conductive structures. Fig. 1 summarizes our approach to create a three-component ink formulation that allows successful DIW printing of spiral antennae on poly(ethylene terephthalate) (PET) illustrating the robustness of the printed structures. We show that a bottom-up approach to CP bulk synthesis, ink formulation, and high-throughput printing with PANI-DNNSA and thermoplastic additives is highly effective and straightforward. Our approach first involves synthesizing PANI-DNNSA, which is then co-dissolved with two rheological modifiers, FS and UHMW-PS in toluene. FS assists in shape retention by increasing yield strength and shear modulus, whereas UHMW-PS aids in manipulating ink viscosity (as a result of a sufficiently high number of entanglements per chain) as well as in enhancing

ductility, robustness, and crack resistance of printed structures. UHMW-PS was selected as it is a highly studied and generalizable commodity thermoplastic that allows us to access exceptionally high molecular weights with low dispersity due to the advantages of anionic polymerization techniques ($> 20,000 \text{ kg mol}^{-1}$). As we consider the role of these two additives, we find that (in a binary system) UHMW-PS has a notably smaller impact on the achievable electrical conductivities of the resulting PANI structures when compared to FS. Additionally, the presence of entanglements between the UHMW-PS and the CP appears to be successful in preventing phase separation of the ink, resulting in the formulation remaining stable for at least a year so that it could be printed with reproducible electrical properties. Post-treatments with low-molecular weight alcohols used for enhancing the conductivity of PANI-DNNSA can also be exploited with our formulations to manipulate the conductivity of printed structures over seven orders of magnitude from 10^{-7} to approximately 10^0 S cm^{-1} .

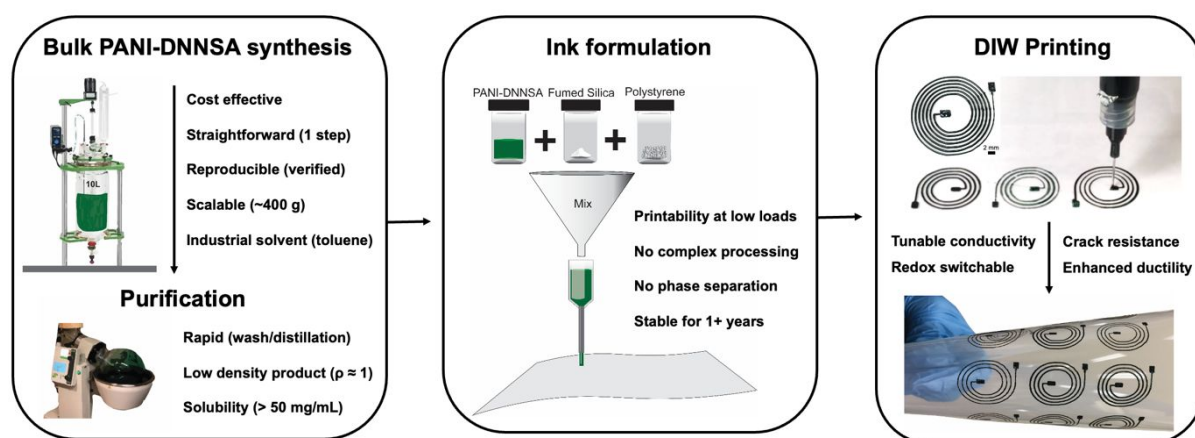


Fig. 1. Overview of bottom-up approach to bulk conducting polyaniline synthesis, purification, ink formulation, and high-throughput DIW printing. Right panel shows photographs of 2-layered spiral antennae printed on PET, before and after bending the substrate with an approximate bend radius of 2 cm. Inset in right panel shows an image of the more complex and larger-size spiral antenna taken from a top-down perspective.

Experimental Methods

All starting materials were purchased from commercial suppliers and used without further purification except aniline, which was distilled prior to use. DNNSA (NACURE 1051) was supplied by King Industries. FFS (0.2 - 0.3 μm particle size, Sigma Aldrich) and UHMW-PS (30,000 kg/mol, $M_w/M_n = 1.3$, Polysciences) were used as rheological modifiers for ink formulation. 5 mL Luer-lock syringes (Nordson EFD) were used as extruders. PANI-DNNSA was synthesized according to published methods.²³ The scale-up procedure used can be found in the Supporting Information.

PANI-DNNSA Synthesis. The synthesis of PANI-DNNSA was carried out using a 10-liter bulk scale reactor vessel (see Fig. S2). One mole of DNNSA (NACURE 1051, as a 50% w/w solution in 2-butoxyethanol), 0.6 moles of aniline, and 2 L of deionized water (purified using a Millipore purification system) were added to the reactor. This resulted in a formation of biphasic liquid-liquid mixture. The mixture was mechanically stirred creating a milky white emulsion. The reaction was then chilled to $-5\text{ }^\circ\text{C}$ and placed under nitrogen. Ammonium persulfate (0.7 mol in 400 mL of water) was used as the oxidant and was added to the mixture in small aliquots over a period of approximately 1 hour. During addition, it was observed that the emulsion changed color from milky white to amber (Figures S2a and S2b). The stirring and cooling were stopped after 17 h and a separation of a green, 2-butoxyethanol phase and a

colorless, aqueous phase was observed. Approximately 500 mL of toluene was added to the reaction vessel and the organic phase was then washed three times with water, leaving a dark-green and highly concentrated PANI-DNNSA solution. Note, while most of the 2-butoxyethanol used in the reaction is removed with aqueous washes, there is likely a residual amount present within the final PANI-DNNSA. This concentrate was readily soluble in xylene, toluene, and hexanes. Three azeotropic distillations were performed on the PANI-DNNSA concentrate by metering in toluene continuously (see Figure S2c) to remove any residual water. According to gravimetric analysis, the yield was approximately 380 grams of PANI-DNNSA, representing an 81% yield based on aniline:DNNSA 1:1.7. Anal. calcd. for $C_{40}H_{54}N_2O_3S$: C (74.73%), H (8.47%), N (4.36%), S (4.99%); Found, C (75.11%), H (8.98%), N (3.92%), S (4.77%).

Ink Formulation. FS nanoparticles (2-6 wt %,) were gradually added and subsequently stirred in cycles to avoid flocculation, which would lead to inhomogeneous inks and batch-to-batch variance. To prepare PANI-DNNSA-FS inks, the FS was metered directly into the PANI-DNNSA solution and did not require prior dissolution. A stock solution of 2 wt% UHMW-PS was prepared by vigorous stirring at 80 °C for 72 hours. The fully solvated UHMW-PS stock was added with concurrent mechanical stirring into PANI-DNNSA solutions to the desired concentration. In the interest of avoiding discontinuous printing, the inks were filtered through a BioVision nylon syringe filter with a pore size of 10 μm . For more viscous ink formulations, a filter with a 25 μm pore size was required. Finally, the inks were loaded into a 5 mL Luer-lock syringe. To remove bubbles and ensure homogenization, the syringes, sealed with a Luer-lock cap, were wrapped with paper towels and put in falcon tubes for centrifuging (1000 – 3000 rpm for 5 - 10 minutes, depending on the viscosity). Further explanation of the necessity of these methods can be found in the Supporting Information.

DIW Printing. DIW printing was performed using a single nozzle home-made DIW printer set up and respective designs produced in Solidworks (Fig. S5, ESI). The extruder (5 mL, luer-lock syringe) is controlled by a pressure regulator (Ultimus V, Nordson EFD) and can be moved in the x- and z-directions, while the printing platform moves in the y-direction. A nozzle with an inner diameter of 0.41 mm (22GA) was affixed to the syringe. The pressure varied between 15-90 psi and the printing speed between 6-10 mm/s depending on the ink viscosity and formulation.

Rheological Characterization. Rheometry was performed using a rotational rheometer (Discovery HR-2, TA Instruments) with a 20-mm-diameter cross-hatched plate geometry at 25 °C with a gap height of 0.5 mm. Viscometry of the PANI and UHMW-PS solutions at different concentrations were measured by a DV2TLV cone and plate viscometer using a CPA-52Z cone spindle (Brookfield Engineering Labs Inc., Middleboro, MA, USA). The sample volume was 0.5 mL. Rheological responses of the materials were characterized using both steady and oscillatory shear methods. Note, steady shear measurements involved the measurement of the torque at discrete shear rates in succession. Before any measurement, samples were pre-sheared at a rate of 1 s^{-1} and allowed to rest for 10 minutes in order to erase any shear history. Apparent viscosities were measured via steady-state flow experiments with a sweep of shear rates ($0.1\text{--}1000 \text{ s}^{-1}$). Shear storage moduli were measured as a function of shear strain via oscillation experiments at a fixed frequency of 1 Hz with a sweep of the strain of (0.02%–5000%). Dynamic mechanical analysis (DMA) tests were conducted on the DMA tester (model Q800, TA Instruments, Inc. New Castle, DE, USA) using a tension clamp under a constant amplitude of 30 μm , frequency of 1 Hz, and force track of 125%.

Electrical Conductivity Measurements. Solid-state electrical conductivity was determined with a standard four-point probe using a van der Pauw geometry. The sheet resistance was

measured using a Keithley 2400 source meter. The sheet resistance, R_s , was calculated using the van der Pauw formula (Fig. S11, ESI). Polymer films were blade-coated with a custom blade coater using a gap height of 100 μm and a blade speed of 30 mm s^{-1} . 1 cm^2 square mats were extruded in a DIW fashion to analyze differences with printed structures. Silver contacts were painted on all four corners of the dry, treated polymer films, and printed square mats. Film thicknesses were measured using a Bruker Dektak XT profilometer. Printed mat thicknesses were determined by optical microscopy and were typically the same as the diameter of the extrusion nozzle (400-450 μm). These prepared samples were dried for at least 72 hours under vacuum at 40 $^\circ\text{C}$ prior to measurements.

Results and Discussion

Ink Formulation Optimization. Our approach to formulate and print the PANI-based inks, and to produce conducting structures through post-deposition solvent treatments, is summarized in Fig. 2. As we will show, post-deposition solvent treatments with isopropanol (IPA) or *n*-butyl alcohol (BuOH) with *p*-toluenesulfonic acid (pTSA) allow us to manipulate electrical conductivity over seven orders of magnitude. We synthesized 380 g of PANI-DNNSA using an emulsion polymerization technique to demonstrate the scalability of the conductive feedstock material (Fig. S2, ESI).²³ The number average molecular weight (M_n) of the polymer was estimated by gel permeation chromatography to be 28 kg mol^{-1} (Fig. S3, ESI). The apparent viscosity of the PANI-DNNSA solutions increases over four orders of magnitude when increasing the concentration from 5 to 50 wt% (Fig. S4, ESI). However, as shown in Fig. 3a,

even at 85 wt% PANI-DNNSA/toluene pastes display a low yield stress and low shear modulus of $\approx 10^1$ Pa, which is far below the 10^3 Pa threshold required for adequate extrusion and shape retention for DIW. Therefore, without additives, these PANI-DNNSA/toluene formulations have insufficient viscosity, low degree of shear-thinning characteristics, and no measurable yield stress due to its relatively low molecular weight, rendering them incapable of holding shape post-extrusion.

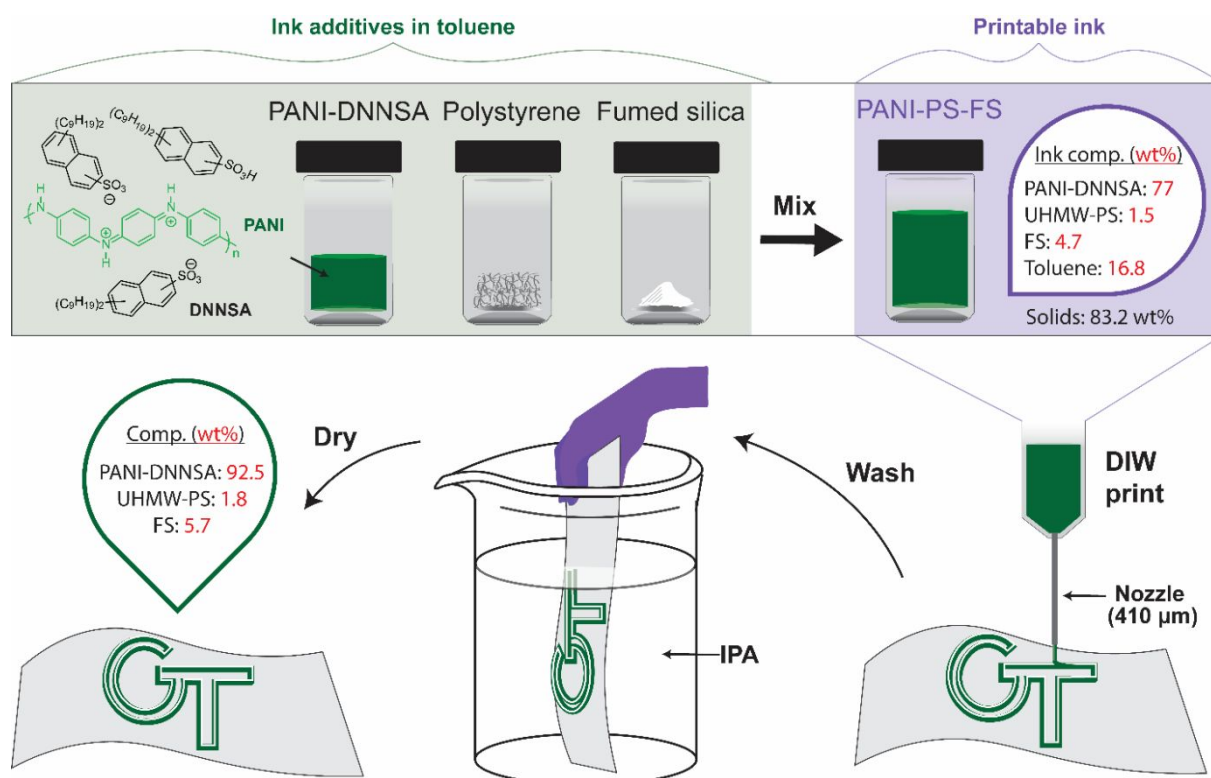


Fig. 2. General procedure for preparing PANI-PS-FS structures with conductivities ranging from $< 10^{-7}$ to 10^0 S cm^{-1} using DIW printing. The chemical structures of the PANI conductor and DNNSA dopant are shown in green and black, respectively, in the top left. PANI-PS-FS ink and printed solid compositions are provided as weight fractions.

To improve the rheological properties of PANI-DNNSA, and thereby making it amenable to DIW, we incorporated FS and UHMW-PS as ink additives. Toluene was chosen as the common solvent to dissolve the PANI-DNNSA, UHMW-PS, and to promote flocculation of FS nanoparticles, which causes the desired increase in viscosity and viscoelastic moduli crucial for printing and shape retention. The superior mixing of the additives and the PANI-DNNSA in toluene is hypothesized to prevent liquid-liquid phase separation of the formulation, which is an essential for obtaining reproducible and stable inks. FS is known to assist in shape retention by increasing yield strength and shear modulus of DIW inks, whereas UHMW-PS can aid in manipulating ink viscosity as even at low compositions. As we will discuss below, thermoplastic additives can offer specific advantages such as improved printability at lower filler content, resistance to cracking, and increased ductility. Here, the organic processability of PANI-DNNSA offers advantages over PEDOT-PSS — namely, because PEDOT-PSS is processed as an aqueous dispersion, it cannot mix with most thermoplastics. By leveraging the organic processability of PANI-DNNSA, we are able to employ UHMW-PS in formulations to demonstrate this concept. Through rigorous ink formulation optimization, we determined a composition of 77 wt% PANI-DNNSA, 1.5 wt% UHMW-PS, 4.7 wt% FS, and 16.8% toluene (all inks prepared with UHMW-PS are labeled “PS” for short in the following sections) provided the best properties to both the ink and the structures created from their printing. More

details on the ink preparation, such as sequence of component addition and mixing times, as well as the chemical structures of the additives can be found on the Supporting Information (Fig. S1, ESI).

As shown in Fig. 3a, PANI-PS-FS is a viscoelastic solid capable of reversible rheological flow behavior that shear thins and flows during extrusion, that rapidly recovers its elastic-like response when contacting the surface to retain the shape, and that has a modulus of 10^3 Pa which is suitable for DIW in a line-by-line and, subsequently, layer-by-layer fashion. In contrast, without the additives, even at concentrations as high as 85 wt% PANI:DNNSA in toluene, the pastes exhibited liquid flow behavior that resulted in spreading of the ink and low-resolution print lines (Fig. 3b). Using the optimized PANI-PS-FS ink, numerous structures such as grids, spiral antennae, square mats, filaments, and a Georgia Tech (GT) logo were printed to demonstrate the quality of printed parts with minimal printing parameter optimization (see Fig. 3c and d, and S6 and S7 in the ESI).

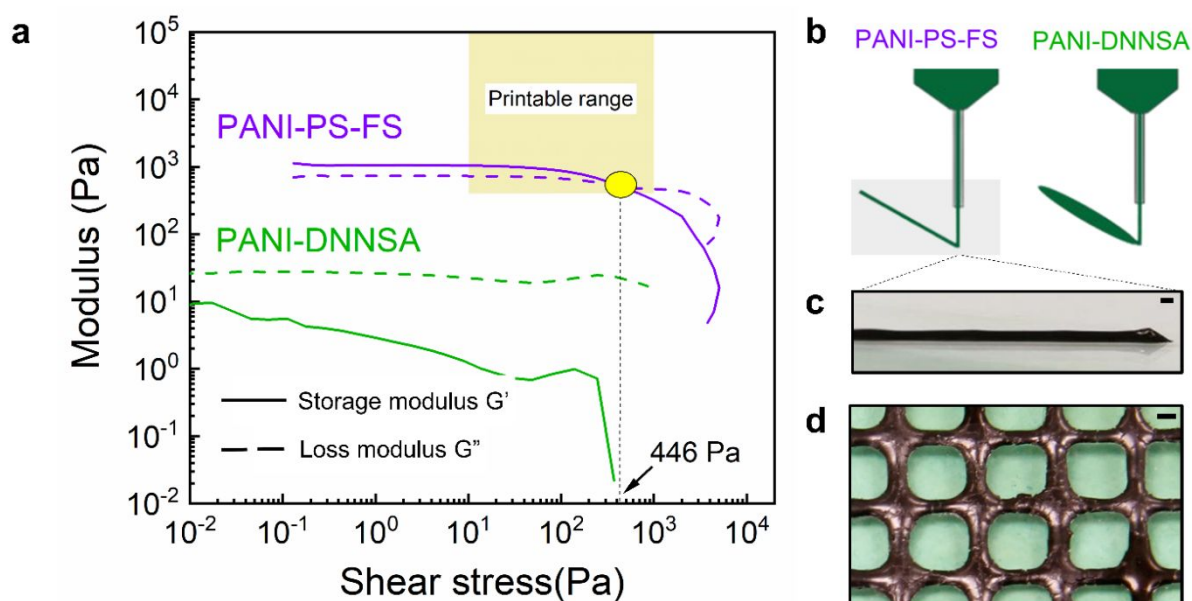


Figure 3. (a) Rheological data of a PANI-DNNSA/toluene solution (85 wt% solids) and PANI-PS-FS ink (77 - 1.5 - 4.7 wt%, respectively) with 83.2 wt% solids comparing storage (G') and loss moduli (G'') as a function of shear stress. A low shear stress ($\tau < 10^{-1}$ Pa) is measured for the neat PANI-DNNSA solutions; i.e., they feature neither a steady-state nor dynamic rheological response that is characteristic of a viscoelastic solid, typified by the storage modulus (G') having a higher value relative to the loss modulus (G'') in the low-stress, linear regime with a characteristic point where G' and G'' crossover (highlighted with a yellow circle) and corresponding to the yield stress. (b) Schematic of the printing process of PANI-PS-FS (purple) and PANI-DNNSA (green) illustrating the spreading of print lines in inks without UHMW-PS or FS. Optical micrographs of (c) a single filament and (d) a DIW printed grid (after a IPA post-treatment) that demonstrate the continuity and homogeneity of PANI-PS-FS printed structures (scale bars = 500 μm). Similar shape fidelity was observed using a BuOH/pTSA treatment.

Additive Effects on Ink Rheology and Conductivity. To delineate the beneficial effects of the FS and the UHMW-PS additives to the ternary ink formulation, and to advance our understanding towards predictive formulation design, we first quantitatively assessed the influence of each additive on the apparent viscosity, shear-thinning, shear-yielding, and shear moduli of the binary PANI-FS and PANI-PS inks (Fig. 4a-d). To be able to compare the

additives within a comparable apparent viscosity and shear moduli range, inks of different PANI-DNNSA content were required to be used (50 wt% with respect to the total ink composition for PANI-FS; 10 wt% for PANI-PS). Therefore, shear-rate sweep measurements were performed on inks of lower solid content than in the optimum ternary ink formulation (77 wt% PANI-DNNSA with respect to the total ink composition).

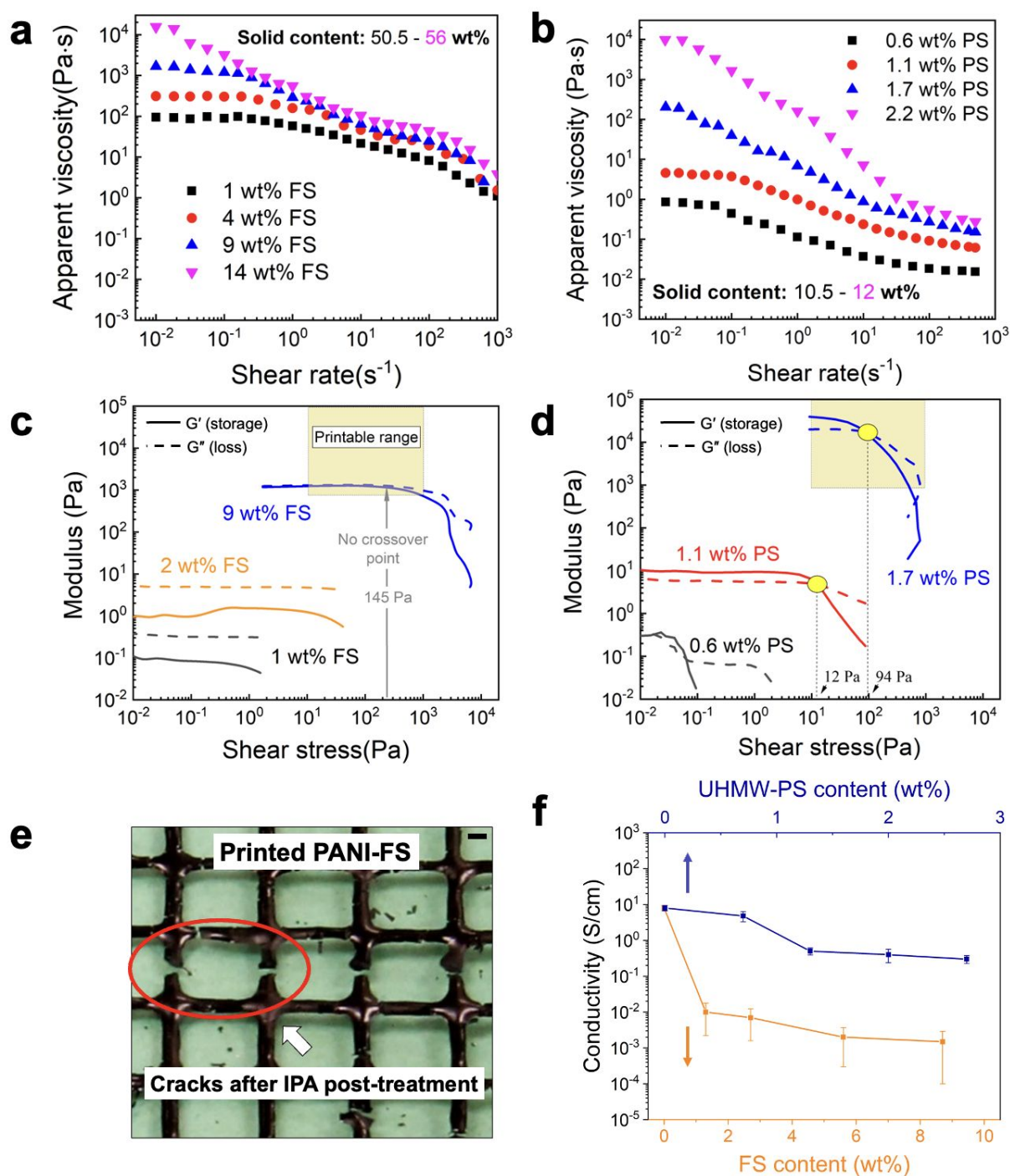


Fig. 4. Comparison of the rheological behavior of (a) PANI-FS and (b) PANI-PS inks using toluene as the solvent. Apparent viscosity as a function of shear rate for varying content of (a) FS and (b) UHMW-PS, using a solid content of 50 and 10 wt% PANI-DNNSA, respectively, for comparable apparent viscosities. The FS content was varied from 1 (black squares), 4 (red circles), 9 (blue triangles), to 14 wt% (purple triangles) with respect to toluene (total solid content from 50.5 to 56 wt%). The UHMW-PS content was varied from 0.6 (black squares), 1.1 (red circles), 1.7 (blue triangles), to 2.2 wt% (purple triangles) corresponding to a total solid

content 10.5 to 12 wt%. Rheological characterizations of CP inks with various additive content of (c) FS and (d) UHMW-PS, using 50 and 10 wt% PANI-DNNSA in toluene, respectively. For these measurements, FS content was varied from 1 (black lines), 2 (orange lines), to 9 wt% (blue lines) with respect to toluene (total solid content of 50.5, 51, and 54 wt%, respectively). UHMW-PS content varied from 0.6 (black lines), 1.1 (red lines), to 1.7 wt% (blue lines) with respect to toluene (total solid content of 10.5, 11, and 11.5 wt%). Storage and loss moduli were determined using a linear stress sweep technique, where shear yield stresses (crossover points) where the two moduli intersect (yellow circle with black dashed line) could be identified for viscoelastic inks. (e) Photograph of DIW-printed PANI-FS ink (50 and 6 wt% of PANI-DNNSA and FS, respectively), which corresponds to a total solid content of 56 wt% , with 14 wt% FS (purple triangles in (a)) with respect to toluene. The two-layer cross-hatch structures printed without UHMW-PS lack mechanical integrity after washing with IPA for 30 s (black scale bar = 1 mm). (f) Solid-state conductivity measured with the van der Pauw method as a function of FS (orange curve) and UHMW-PS (blue curve) content after a 30 s IPA post-treatment with IPA.

Fig. 4a and 4b compares the rheological behavior of the binary PANI-FS and PANI-PS inks, respectively. For PANI-FS we observe an increase in the apparent viscosity from 10^2 to 10^4 Pa·s at a low shear rate of 10^{-2} s $^{-1}$ when increasing the fraction of FS in the formulations from 1 to 14 wt% (w.r.t. toluene). At higher shear rates above 10^3 s $^{-1}$, the apparent viscosity of PANI-FS inks reach a plateau around $0.5 - 1 \times 10^1$ Pa·s. Note, as Fig. 4c illustrates, PANI-FS binary inks do not reach a cross-over point, *i.e.*, they do not have a yield stress, due to the loss modulus remaining higher than the storage modulus in the lower shear rate regime, which indicates more liquid-like flow behavior — an indication that this binary would result in spreading during DIW printing. For binaries with 14 wt% FS with respect to toluene, the apparent viscosity

enhancement at low shear rates comes with a concomitant increase of the yield stress up to 200-300 Pa (not shown), which allowed for the DIW printing of multilayer cross-hatch structures, as the photograph in Fig. 4e shows. However, while we were able to successfully print multilayer cross-hatch structures using this ink, during the post-treatment step where the PANI-FS printed structures were rinsed with IPA to remove excess DNNSA, we observed undesirable cracking caused by drastic shrinkage of the printed structures.

In contrast, the PANI-PS binaries exhibited a cross-over point at just 1.7 wt% additive concentration. These binaries, while in the regime for printability, led to structures with non-ideal shape retention, presumably due to their relatively low yield stresses < 90 Pa. For the PANI-PS binaries, a significant increase in the apparent viscosity of the inks was measured as a function of relatively subtle changes in UHMW-PS content from below 10^0 Pa·s to above 10^4 Pa·s at a shear rate of 10^{-2} s $^{-1}$ when increasing the concentration of UHMW-PS from 0.6 wt% to 2.2 wt% in toluene (Fig. 4b). Additionally, Fig. 4d shows an increase in the viscoelastic moduli from less than 10^0 to more than 10^4 Pa at a shear stress of 10^{-2} Pa for PANI-PS inks with 0.6 and 1.7 wt% UHMW-PS, respectively. Conversely, the poor shape-retention of inks with low UHMW-PS content led to poor DIW printing resolution, which is further attributed to these PANI-PS inks having drastically lower yield strengths (12 Pa for 1.1 wt% of PS compared to

~200 Pa for 9 wt% of FS in toluene), as shown in Fig. 4d. Notably, the cracking observed for the IPA treated and dried PANI-FS structures was not observed for that of the PANI-PS structures. Though, shape retention was shown to be an issue for PANI-PS printed parts, the optimization of which with ternary inks will now be discussed.

In addition to comparing the effects on rheological properties, we also evaluated the effect the additives have on the conductivity of the printed structures. As is depicted in Fig. 4f (orange trace), the addition of just a small fraction of FS leads to a decrease in conductivity, from 10^1 S cm^{-1} for the structures printed from neat PANI-DNNSA/toluene inks to $10^{-2} \text{ S cm}^{-1}$ when adding > 1.5 wt% FS with respect to toluene (for reference, this corresponds to 6 wt% FS vs. PANI-DNNSA). The addition of UHMW-PS as a single additive, on the other hand, did not significantly affect the electrical conductivity of printed structures (Fig. 4f, blue trace). From these results, we conclude that only an ink incorporating both FS and UHMW-PS as additives will allow for effective printing. By optimizing the additive concentrations we can then eliminate nozzle clogging and provide shape retention to the printed parts, while also increasing the modulus and elastic properties of the ink. By introducing just 2.2 wt% of UHMW-PS (with respect to toluene) into the PANI-FS formulations, the crack resistance is notably increased in

the printed and IPA post-treated structures, as shown by optical microscopy (Fig. S8, S9, and S10, ESI).

Polymer Entanglement Effects on Ink Rheology. Understanding and controlling the effects of polymer entanglements on ink rheology when using thermoplastics as additives is crucial for successful DIW printing. The concentration and molecular weight at which each polymer chain is entangled with at least two other chains refers to the regime where polymers form a three-dimensional network of entanglements, which begins dominating the viscoelastic properties. Polymer solution theory states there is a critical overlap concentration of polymer chains (C^*), where concentrations higher than C^* result in an increasing number of entanglements.³⁹ Consequently, especially in the case of high molecular weight polymers, subtle increases in the concentration above C^* result in a large enhancement in the ink viscosity (Fig. 5, blue region).⁴⁰⁻⁴² As shown in Fig. 5, microcapillary viscometry allowed us to optimize the concentration for the 30,000 kg/mol UHMW-PS in the inks, as too many entanglements leads to excessively high viscosities and subsequent nozzle clogging, while too few resulted in issues with shape retention. In our inks, the printing nozzles tended to clog because of high viscosity at a content of UHMW-PS > 2 wt% with respect to toluene, while poor shape retention was typically observed < 1.5 wt% UHMW-PS.

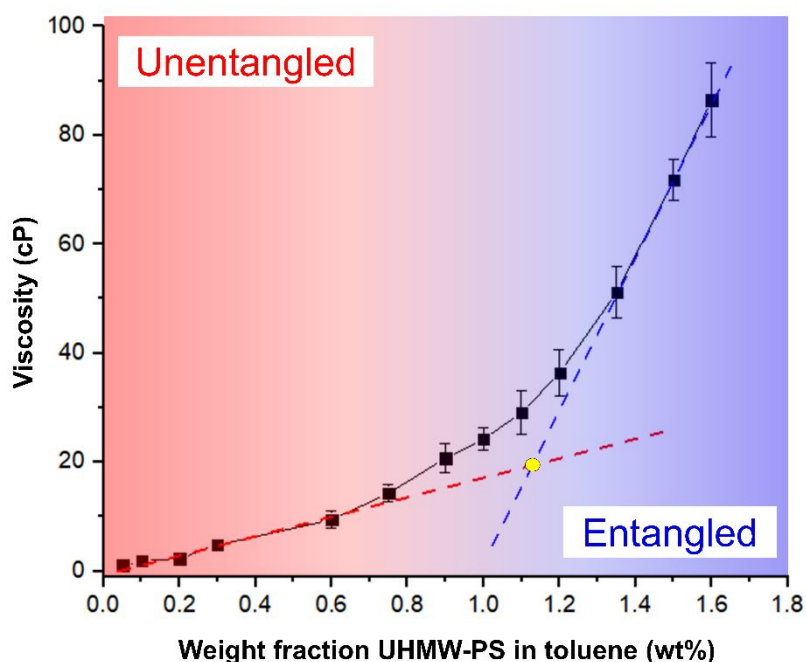


Figure 5. Viscometry of UHMW-PS ($M_w \approx 30,000$ kg/mol) in toluene at varying polymer content allows for the identification critical concentration regimes where the polymer chains entangle (highlighted in blue) leading to an increase in viscosity, vs. a regime where chains do not entangle and predominantly are isolated (red). The color gradient is used to illustrate the semi-dilute regime where chains are partially unentangled and entangled (0.6-1.25 wt%).

An additional advantage of using high molecular weight thermoplastics is that they can form entanglements, which hinder mass transport and can thereby prevent phase separation of ink components and afford inks with a longer shelf-life. Indeed, in contrast to the PANI-FS binary inks, the ternary PANI-PS-FS inks did not phase separate (*i.e.*, no observed liquid-liquid or liquid-solid phase separation) and remained well-mixed and homogeneous for at least a year. This further suggests that, at these higher polymer additive concentrations, entanglements form

between UHMW-PS chains, limiting mass transport and hence phase separation. The lack of phase separation in PANI-PS-FS inks is noteworthy and highlights the effectiveness of introducing entanglements between the polymeric blend components to improve ink stability. This prevention of phase separation also allowed us to test the conductivity of structures produced using the aged inks. Fig. 6a illustrates the performance stability of structures produced from the optimized ink aged under ambient laboratory conditions for up to one year. Each data point represents the average conductivity measured on square mat patterns of at least three 1 cm² squares, which were post-treated and dried *in vacuo* at room temperature. To ensure precision of the conductivity measurements, a van der Pauw method was used to measure all printed samples, the details of which are described and depicted further in the Supporting Information (Fig. S11, ESI). Remarkably, after aging the inks for more than a year, only small changes in conductivity were measured in printed PANI-PS-FS structures, which we attribute to the stability of the ink induced by the presence of the UHMW-PS.

Conductivity Tuning via Post-Print Processing. While printability and stability do come at the expense of the conductivity that can be reached, we are still able to tune the conductivity of the printed structures by over seven orders of magnitude from $< 10^{-7}$ S cm⁻¹ for as-produced structures up to $\sim 10^0$ S cm⁻¹ by varying the post-treatment solvent and the treatment time (Fig.

6b). We find that the BuOH/pTSA wash enhances the conductivity of PANI structures approximately ten-fold compared to structures treated with IPA. We hypothesize that the BuOH/pTSA rinse is not only capable of removing excess DNNSA, as is the case for the IPA treatment, but also allows for dopant exchange where the smaller pTSA molecules replace the bulkier DNNSA, further improving the electrical conductivity. This is in agreement with the hypothesis put forward by Kinlen et al.²³Error! Bookmark not defined. In order to quantify the impact of the IPA and BuOH/pTSA post-treatments on the chemical composition of PANI-DNNSA, we performed X-ray photoelectron spectroscopy (XPS) experiments as shown in Fig. 6c. High-resolution scans were performed for the carbon (1s), nitrogen (1s), and sulfur (2p) binding energy regions, as shown in Fig. S12 (ESI). Additional details on XPS data collection, analysis, elemental spectra, and peak deconvolution are provided in the Supporting Information. Peak areas determined from the nitrogen and sulfur species present were used to determine the doping ratio of the PANI (imine and amine cation versus total nitrogen) and how much excess dopant is present in the film before and after post-treatments, which is illustrated in Fig. 6c. The N^+/N ratio gives us an accurate estimation of the doping level (i.e., number of charges per ring). The N^+/N ratio of the as-synthesized PANI-DNNSA was 0.52, which confirms that the PANI was in the conductive, doped emeraldine state with approximately one charge per every two rings. Rinsing with IPA or BuOH/pTSA decreases this ratio to 0.31 and 0.32, respectively, indicating

that there is dedoping of the PANI occurring during the post-treatment steps. Despite the lower doping level, the removal of excess non-conducting DNNSA results in a higher measured electrical conductivity. By comparing the S/N and S/N+ ratios we obtain an estimation of the amount of excess dopant present in the film. These results corroborate the 2:1 sulfonic acid to aniline ratio approximation determined by elemental analysis for the as-synthesized PANI-DNNSA. Furthermore, the decrease in the S/N ratios for treated films (Fig. 6c) quantitatively shows the removal of DNNSA. IPA and BuOH are, therefore, both sufficiently polar to dissolve the primary dopants, DNNSA and pTSA, without solubilizing the PANI, UHMW-PS, or FS. However, BuOH is crucial in facilitating efficient exchange between the pTSA and DNNSA. The slightly less polar BuOH preferentially dissolves the more apolar dopant, DNNSA, which shifts the equilibrium such that more pTSA remains in the structures.

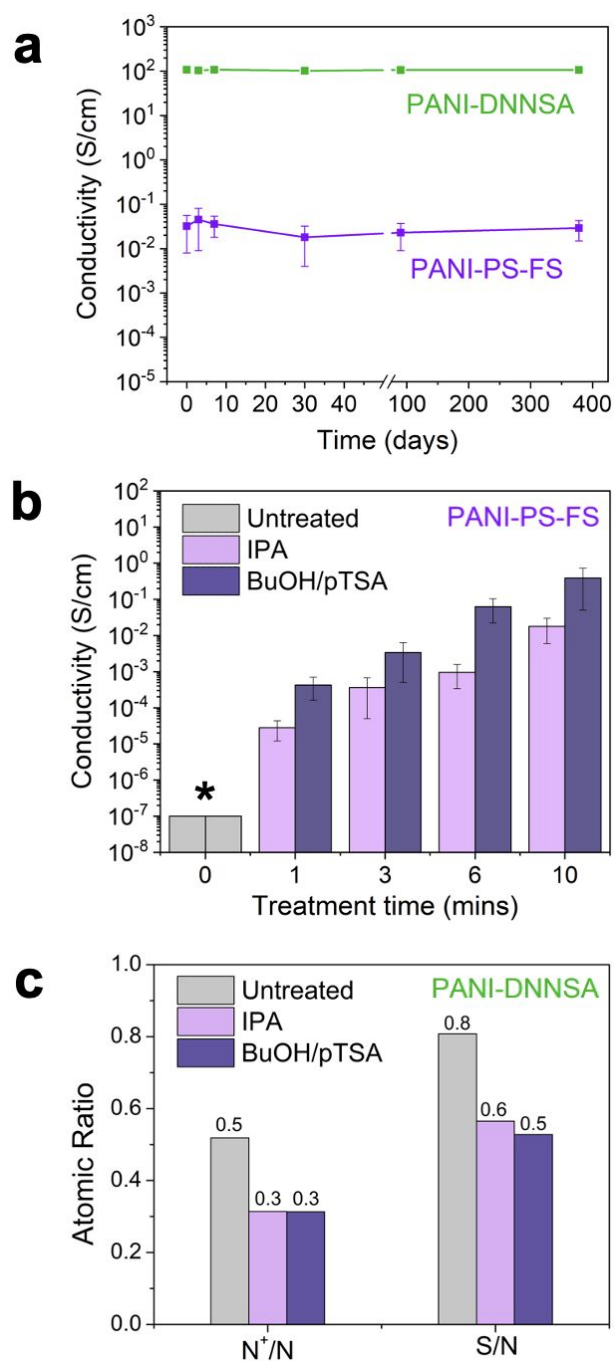


Fig. 6. (a) Solid-state electrical conductivity of extruded and dried structures produced using 50 wt% PANI-DNNSA without additives (green curve) and the final PANI-PS-FS ink formulation (purple curve) after 3 minutes of BuOH/pTSA post-treatment, as a function of the age of the ink after formulation. (b) Solid-state conductivity as a function of post-treatment time for extruded and dried optimized PANI-PS-FS ink. Conductivity was measured on 1 cm^2 PANI-PS-FS mats as a function of IPA (left, pink bar) or BuOH/pTSA (right, purple bar) treatment time (error bars indicate standard deviations). The star (*) represents a minimum conductivity (maximum resistance) value that can be measured by the instrument. All electrical

conductivities were measured using the van der Pauw method. The highest average conductivity with the associated standard deviation was measured for the printed and BuOH/pTSA treated (treatment time = 10 min) PANI-PS-FS structures, which was $0.39 \pm 0.29 \text{ S cm}^{-1}$. (c) Atomic ratios from integrated, deconvoluted high-resolution XPS spectra for pristine PANI-DNNSA N(1s) and S(2p).

Fig. 6b confirms that longer treatment times lead to an increase in the electrical conductivity of our optimized ink formulation. These observations suggest that the conductivity enhancement is limited by the diffusion rate of solvated DNNSA ions into and out of the extruded bulk structures, impacting the process of dopant removal and exchange. Nonetheless, the data highlights that DIW printed PANI-PS-FS structures can access conductivity values that span greater than seven orders of magnitude from less than $10^{-7} \text{ S cm}^{-1}$ for as-produced structures to 10^0 S cm^{-1} after specific post-treatments. This wide range of conductivities is accessible and realized by modifying the dopant, post-treatment time, and redox state of CPs, making this ink formulation useful for applications such as ESD coatings and interfaces.^{1,43} While not being the primary focus of this work, Fig. S13 and S14 (ESI) show that the redox activity of post-treated PANI-PS-FS structures is essentially identical to that of PANI-DNNSA. This ability to reversibly switch printed CP structures between their conductive (oxidized) and insulating (reduced) state allows simultaneous and respective ion uptake and expulsion of the

surrounding electrolyte, which further broadens their impact to geometrically tailorable DIW structures for controlled release, sensors, and electrochemical energy storage applications.⁴⁴⁻⁴⁹

Thermal and Mechanical Properties of Printed Structures. The mechanical, thermal, and thermomechanical properties of PANI-PS-FS printed structures are important to assess the applicability of ink formulations and printed structures for tailored applications. First, varying dynamic mechanical analysis (DMA) tests were attempted on PANI-DNNSA, PANI-FS, and PANI-PS-FS filaments; however, both the PANI-DNNSA and PANI-FS filaments were too brittle for mechanical analysis. The PANI-PS-FS filaments, on the other hand, exhibited enhanced robustness and ductility (> 10% strain at break), as shown in Fig. S15 (ESI). Second, as illustrated by the results in Fig. 7, thermomechanical measurements were performed by comparing DMA results with electrical conductivity data obtained on a printed PANI-PS-FS mat as a function of temperature. From this thermomechanical data, we see a clear thermal transition at approximately 96 °C, which corresponds to an observed yielding of the filament as shown by the crossover point in Fig. 7.

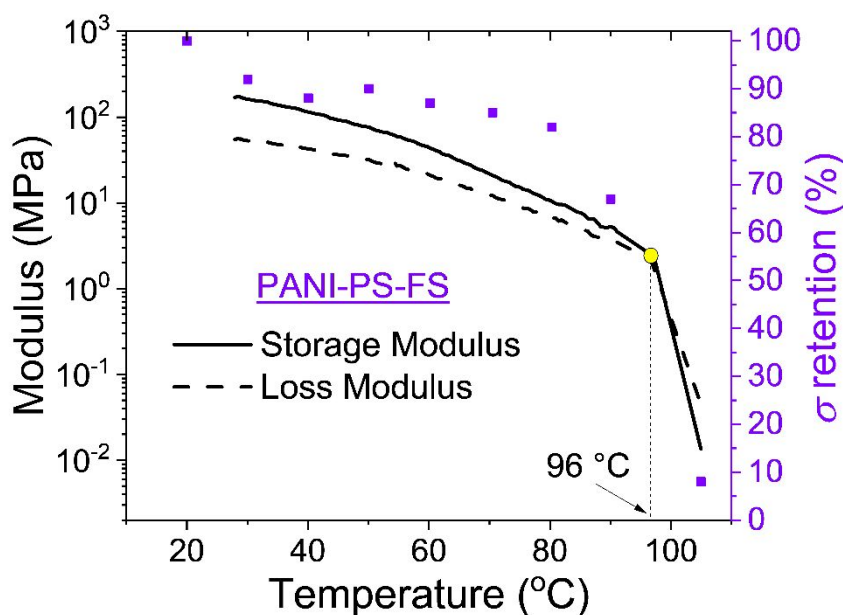


Figure 7. Storage modulus, loss modulus, and solid-state conductivity retention as a function of temperature of a printed PANI-PS-FS filament. Storage and loss moduli were determined using DMA. The temperature sweep for mechanical testing was performed from 25 to 110 °C at a heating rate of 3 °C min⁻¹. Yield point for the filament was identified where the two moduli intersect (yellow circle with dashed line). The electrical conductivity was measured in ≈ 10 °C increments (purple points) using a van der Pauw method (see Fig. S11 and Supporting Information for more details).

Differential scanning calorimetry (DSC) of UHMW-PS (Fig. S16, ESI) estimates the glass transition temperature to be approximately 103 °C, indicating that this response might be due to the softening of the UHMW-PS component. Other possible origins of this thermal transition could be related to the breaking of hydrogen bonds between the hydroxyl groups on the FS surface and the sulfonic acid groups on the DNNSA. Thermogravimetric analysis (TGA, Fig. S17a, ESI) of the dried PANI-PS-FS structures show no weight loss at temperatures below 200 °C, which means we can exclude the possibility of water retention in the solid structures after the drying process. The TGA data also shows that degradation of the printed PANI-PS-FS structures does not occur until approximately 300 °C. The heating traces of printed PANI-PS-FS (Fig. S17b, ESI) show a similar glass transition around 90 °C, which is absent in the PANI-DNNSA heating curves, providing further evidence this transition originates from UHMW-PS

softening. Around the temperature where the PS fraction softens, there is also a notable drop in electrical conductivity from 0.25 to 0.02 S cm⁻¹ for PANI-PS-FS mats measured at 20 and 105 °C, respectively. A similar decrease in electrical conductivity has been previously reported for PANI blends with insulators when annealed at temperatures near or above the T_g of the insulating polymer.⁵⁰ For applications/structures requiring higher annealing temperatures, other commodity polymers with a higher T_g can be employed as long as they are of similar solubility in the solvents used in our process. However, from the point of view of reformability and reusability of printed structures, incorporating thermoplastics with lower T_g could prove to be advantageous.

3. Conclusions and perspective

The data presented in this work show that blending a conducting polymer with an insulating thermoplastic, combined with specific processing aids, is a promising route to print structures of a broad range of electrical conductivities. Specifically, we found that both fumed silica and UHMW-polystyrene are capable of enhancing the viscosity and shear thinning nature of the inks. We opted to incorporate UHMW-PS in inks to highlight the utility of UHMW thermoplastics in crack prevention and rheological tuning of printed, hierarchical structures. Without the addition of UHMW-PS, printed structures readily shrank and formed cracks after post-treatments and were even too brittle for DMA. Conversely, we were unable to print PANI-based inks without FS as binary PANI-PS inks with low PS content (< 1.5 wt% UHMW-PS) resulted in printed structures with poor shape-retention due to low viscosities, whereas inks with a higher PS fraction (> 2 wt% UHMW-PS) clogged the print nozzles because of exceedingly high viscoelastic moduli. While the issues with the rapid increase in viscosities and yield stresses for inks with higher UHMW-PS content may be mitigated by using PS of a lower

molecular weight, this may affect the capability of the thermoplastic to provide structures with excellent shape-retention, ductility, and crack resistance at low loads. Introduction of both FS aggregates and UHMW-PS entanglements were highly successful for manipulating the rheology of the inks. Importantly, UHMW-PS showed exceptional retention of the electrical conductivity of printed structures compared to FS, which further demonstrates the utility of this approach.

By using a ternary ink composition, we demonstrate the ability to not only print robust structures, but also to leverage post-treatments to tune the electrical conductivity. Treatments as short as 10 min increased the conductivity of printed structures significantly, allowing us to reproducibly access a conductivity range of DIW printed structures of over seven orders of magnitude ($<10^{-7} - 10^0$ S cm⁻¹). These conductivities are within values to be considered for EMI and ESD applications. Additionally, the printed PANI-FS-PS structures remained redox active, justifying further studies evaluating these inks for charge storage, strain gauge, and sensing applications. Considering that the ternary ink formulations are remarkably stable – characterized by their resistance to phase separation and the retention of their electrical conductivities (post-printing and processing) over long periods of time exceeding one year – we conclude that the judicious selection of commodity thermoplastic additives and their concentrations is a versatile and straight-forward pathway towards DIW printable inks capable of producing designs with unique electrical, mechanical, and thermal properties. The concept is especially promising for PANI-DNNSA, which is easily synthesized in bulk, processable, and compatible with a range of organic soluble polymers and/or additives. Hence, this approach will contribute to the ongoing effort of bringing the promising properties of CPs to the future of structural electronics.

Conflicts of interest

There are no conflicts to declare.

Acknowledgements

This work was supported by the National Science Foundation under Grant No. IIP-#1822141 (Phase I IUCRC at Georgia Institute of Technology: Center for Science of Heterogeneous Additive Printing of 3D Materials (SHAP3D) and from the SHAP3D I/UCRC Members: Akita Innovations, Boeing Company, U.S. Army CCDC Armaments Center, U.S. Army CCDC Soldier Center, Desktop Metal, HP Inc, Hutchinson, Integrity Industrial Ink Jet Integration LLC, Karagozian & Case, Raytheon Technologies, Stratasys Ltd, and Triton Systems Inc. Any opinions, findings, and conclusions or recommendations expressed in this work are those of the author(s) and do not necessarily reflect the views of the National Science Foundation or the sponsors. The authors acknowledge Prof. Blair Brettmann's lab for the shared rheology instrumentation. Brandon T. DiTullio acknowledges the support by the Department of Defense (DoD) through the National Defense Science & Engineering Graduate (NDSEG) Fellowship program. The authors thank Justin Speregen for his help with rheology and conductivity measurements. This work was performed in part at the Georgia Tech Institute of Electronics and Nanotechnology, a member of the National Nanotechnology Coordinated Infrastructure, which is supported by the National Science Foundation (grant ECCS1542174). Thermal characterizations were performed at the Organic Materials Characterization Laboratory at Georgia Tech.

Footnotes

Electronic supplementary information (ESI) available.

References

1. P. Saini, V. Choudhary and S. K. Dhawan, *Polym. Adv. Technol.*, 2012, **23**, 343-49.
2. J. Lyu, X. Zhao, X. Hou, Y. Zhang, T. Li and Y. Yan, *Compos. Sci. Technol.*, 2017, **149**, 159-165.
3. F. Fang, Y.-Q. Li, H.-M. Xiao, N. Hu and S.-Y. Fu, *J. Mater. Chem. C* 2016, **4**, 4193-4203.
4. O. Yarimaga, J. Jaworski, B. Yoon and J.-M. Kim, *Chem. Commun.*, 2012, **48**, 2469-85.
5. A.-D. Bendrea, L. Cianga and I. Cianga, *J. Biomater. Appl.*, 2011, **26**, 3-84.
6. F. Hu, Y. Xue, J. Xu and B. Lu, *Front. Robot. AI*, 2019, **6**, 114.
7. Q.-W. Wang, H.-B. Zhang, J. Liu, S. Zhao, X. Xie, L. Liu, R. Yang, N. Koratkar and Z.-Z. Yu, *Adv. Funct. Mater.*, 2018, **29**, 1806819.
8. Y. Luo, R. Guo, T. Li, F. Li, Z. Liu, M. Zheng, B. Wang, Z. Yang, H. Luo and Y. Wan, *ChemSusChem*, 2018, **12**, 1591-1611.
9. S. Tagliaferri, A. Panagiotopoulos and C. Mattevi, *Mater. Adv.*, 2021, **2**, 540-563.
10. R. Megha, F. A. Ali, Y. T. Ravikiran, C. H. V. V. Ramana, A. B. V. Kiran Kumar, D. K. Mishra, S. C. Vijayakumari and D. Kim, *Inorg. Chem. Commun.*, 2018, **98**, 11-28.
11. C. Cochrane, M. Lewandowski and V. Koncar, *Sensors*, 2010, **10**, 8291-8303.
12. T. M. Swager, *Macromolecules*, 2017, **50**, 4867-4886.
13. B. J. Worfolk, S. C. Andrews, S. Park, J. Reinspach, N. Liu, M. F. Toney, S. Mannsfeld and Z. Bao, *Proc. Natl. Acad. Sci. U.S.A.*, 2015, **112**, 14138-14143.
14. X. Wang, X. Zhang, L. Sun, D. Lee, S. Lee, M. Wang, J. Zhao, Y. Shao-Horn, M. Dinca, T. Palacios and K. Gleason, *Sci. Adv.*, 2018, **4**, 1-10.
15. B. P. Conner, G. P. Manogharan, A. N. Martof, L. M. Rodomsky, C. M. Rodomsky, D. C. Jordan and J. W. Limperos, *Additive Manufacturing*, 2014, 1-4, 64.

-
16. H. Yuk, B. Lu, S. Lin, K. Qu, J. Xu, J. Luo and X. Zhao, *Nat. Comm.*, 2020, **11**, 1604.
 17. D. N. Heo, S.-J. Lee, R. Timsina, X. Qiu, N. Castro and L. G. Zhang, *Mater. Sci. Eng. C Mater. Biol. Appl.*, 2019, **99**, 582-590.
 18. Z. Wang, Q. Zhang, S. Long, Y. Luo, Y. Peikai, Z. Tan, J. Bai, B. Qu, Y. Yang, J. Shi, H. Zhou, Z.-Y. Xiao, W. Hong and H. Bai, *ACS Appl. Mater. Interfaces*, 2018, **10**, 10437-10444.
 19. B. Holness and A. Price, *Smart Mater. Struct.*, 2017, **27**, 015006.
 20. A. Eftekhari, L. Li and Y. Yang, *J. Power Sources*, 2017, **347**, 86-107.
 21. I. Fratoddi, I. Venditti, C. Cametti and M. Russo, *Sensor. Actuat. B-Chem.*, 2015, **220**, 534-548.
 22. T. Qazi, R. Rai and A. Boccaccini, *Biomaterials*, 2014, **35**, 9068-86.
 23. P. J. Kinlen, J. Liu, Y. Ding, C. R. Graham and E. E. Remsen, *Macromolecules*, 1998, **31**, 1735-1744.
 24. Y. Ding, S. Hayes and J. C. Simpson (Lumimove, Inc., A Missouri Corporation, DBA Crosslink) *US 011621*, **2007**.
 25. H. Yang, D. Kim, A. K. Singh, B. W. Pitts, G. J. Tregre and P. J. Kinlen, *MRS Proceedings*, 2011, **1312**, DOI 10.1557/opl.2011.907.
 26. V. G. Rocha, E. Saiz, I. S. Tirichenko and E. García-Tuñón, *J. Mater. Chem. A*, 2020, **8**, 15646-15657.
 27. Y. Zhang, G. Shi, J. Qin, S. E. Lowe, S. Zhang, H. Zhao and Y. L. Zhong, *ACS Appl. Electron. Mater.*, 2019, **1**, 1718-1734.
 28. M. L. Bedell, A. M. Navara, Y. Du, S. Zhang and A. G. Mikos, *Chem. Rev.*, 2020, **120**, 10744-10792.

-
29. J. Kim, R. Kumar, A. J. Bandodkar and J. Wang, *Adv. Electron. Mater.*, 2017, **3**, 1600260.
 30. A. M'Barki, L. Bocquet and A. Stevenson, *Sci. Rep.*, 2017, **7**, 6017.
 31. M. R. Sommer, L. Alison, C. Minas, E. Tervoort, P. A. Rühls and A. R. Studart, *Soft Matter*, 2017, **13**, 1794-1803.
 32. A. Corker, H. C.-H. Ng, R. J. Poole and E. García-Tuñón, *Soft Matter*, 2019, **15**, 1444-1456.
 33. N. Isabeta and B. Biscans, *Powder Technology*, 2010, **203**, 206-210.
 34. Z. Miao, J. Seo and M. A. Hickner, *Polymer*, 2018, **152**, 18-24.
 35. H. Wei, M. Lei, P. Zhang, J. Leng, Z. Zheng and Y. Yu, *Nat. Comm.*, 2021, **12**, 2082.
 36. A. C. Arias, F. Endicott and R. A. Street, *Adv. Mater.*, 2006, **18**, 2900-2904.
 37. S. Goffri, C. Müller, N. Stingelin-Stutzmann, D. W. Breiby, C. P. Radano, J. W. Andreasen, R. Thompson, R. A. J. Janssen, M. M. Nielsen, P. Smith and H. Sirringhaus, *Nat. Mater.*, 2006, **5**, 950-956.
 38. T. A. M. Ferenczi, C. Müller, D. D. C. Bradley, P. Smith, J. Nelson and N. Stingelin, *Adv. Mater.*, 2011, **23**, 4093-4097.
 39. Q. C. Ying and B. J. Chu, *Macromolecules*, 1987, **20**, 362.
 40. W. G. Graessley, in *The Entanglement Concept in Polymer Rheology. Advances in Polymer Science*, Vol. 16, Springer, Berlin, Heidelberg 1974.
 41. F. Bueche, *J. Chem. Phys.*, 1952, **20**, 1959.
 42. C. Tsenoglou, *Macromolecules*, 2001, **34**, 2148-2155.
 43. P. Saini and V. Choudhary, *Indian J. Pure Ap. Phy.*, 2013, **51**, 112-117.

-
44. A. M. Bryan, L. M. Santino, Y. Lu, S. Acharya and J. M. D'Arcy, *Chem. Mater.*, 2016, **28**, 5989-5998.
45. P. Beaujuge and J. R. Reynolds, *Chemical Reviews*, 2010, **110**, 268-320.
46. H. Park, Y. R. Jeong, J. Yun, S. Y. Hong, S. Jin, S. Lee, G. Zi and J. S. Ha, *ACS Nano*, 2015, **9**, 9974-9985.
47. C. O. Baker, X. Huang, W. Nelson and R. B. Kaner, *Chem. Soc. Rev.*, 2017, **46**, 1510.
48. D. Svirskis, J. Travas-Sejdic, A. Rodgers and S. Garg, *J. Control. Release*, 2010, **146**, 6-15.
49. J. H. T. Luong, T. Narayan, S. Solanki and B. D. Malhotra, *J. Funct. Biomater.*, 2020, **11**, 71.
50. J. Frayasse, J. Planes and A. Dufresne, *Mol. Cryst. Liq. Cryst.*, 2000, **354**, 1099.